Determination of heterogeneous reaction mechanisms: A key milestone in dust explosion modelling

Matteo Pietraccini, Eloise Delon, Audrey Santandrea, Stéphanie Pacault, Pierre-Alexandre Glaude, Anthony Dufour, Olivier Dufaud

Determination of heterogeneous reaction mechanisms: a key milestone in dust explosion modeling

Matteo Pietraccini [a], Eloise Delon [a], Audrey Santandrea [a], Stéphanie Pacault [a], Pierre-Alexandre Glaude [a], Anthony Dufour [a] & Olivier Dufaud [a]

[a] Université de Lorraine, CNRS, LRGP, F-54000 Nancy, France

E-mail: *olivier.dufaud@univ-lorraine.fr*

Abstract

Reaction kinetics is fundamental for modelling the thermal oxidation of a solid phase, in processes such as dust explosions, combustion or gasification. The methodology followed in this study consists in i) the experimental identification of the reaction mechanisms involved in the explosion of organic powders, ii) the proposal of simplified mechanisms of pyrolysis and oxidation, iii) the implementation of the model to assess the explosion severity of organic dusts. Flash pyrolysis and combustion experiments were carried out on starch (22 µm) and cellulose (53 µm) at temperatures ranging from 973K to 1173K. The gases generated were collected and analyzed by gas chromatography. In this paper, a semi-global pyrolysis model was developed for reactive systems with low Damköhler number. It is in good agreement with the experimental data and shows that both carbon monoxide and hydrogen are mainly generated during the pyrolysis of the solid, the generation of the latter compound being greatly promoted at high temperature. A simplified combustion model was also proposed by adding two oxidation reactions of the pyrolysis products. In parallel, flame propagation tests were performed in a semi open tube in order to assess the burning velocity of such compounds. The laminar burning velocity of cellulose was determined to be 21 $cm.s^{-1}$. Finally, this model will be integrated to a predictive model of dust explosions and its validation will be based on experimental data obtained using the 20 L explosion sphere. The

explosion severity of cellulose was determined and will be used to develop and adjust the predictive model.

Keywords: *pyrolysis, combustion, dust explosion, organic powders, reaction mechanisms*

1. Introduction

The importance of merging process safety and engineering design together is well known; but if inherent safety is essential (Rathnayaka et al., 2014), it is also compulsory to complement this approach by the quantitative assessment of residual risks. However, for dust explosion as for other risks, the industrial conditions are multiple, changing and can hardly be reproduced in a laboratory by a series of experiments. Supporting the tests with a numerical model able to extrapolate their results to operating conditions other than those defined by the international standards, would obviously increase the relevance and scope of a normative approach.

Developing such a model is far from being easy as various steps have to be considered: for instance, i) the dust dispersion and the potential variation of its particle size distribution, ii) the dust ignition, which is by nature a discontinuous process, iii) the flame propagation and the turbulence/combustion interactions. Among the essential bricks of this model, the chemical reaction kinetics is probably the most central input. However, at present, the proposed reaction mechanisms do not allow to represent the complexity of these phenomena. Indeed, predictive models of solid combustion exist, but are almost always based on slow heating tests of powder deposits, such as thermo-gravimetric analysis (Liu et al., 2019; Zhang et al, 2020). In such cases, both particle heating rate and transport phenomena lead to models which cannot represent accurately neither the heterogeneity of a dust cloud, nor its reaction limitations. Regarding the last point, some predictive models were proposed assuming that the explosion severity of a dust is mainly related to the heat transfer phenomena rate, which allows the development of kinetic-free models (Fumagalli et al., 2018; Scotton et al., 2020). However, although they seem to give satisfactory results, they are limited to large particles whose reactivity is limited by the external heat transfer. For small

52 particles, or powders with a large PSD including small particles, their explosion severity cannot be
53 dissociated from their combustion kinetics. In order to model a dust explosion phenomenon or/and a
54 gasification process it is thus compulsory to determine the rate-limiting mechanisms occurring
55 during the rapid heating of a dust cloud, followed by a flash pyrolysis and an oxidation step. In such
56 a way, not only a dust explosion could be mathematically described, but a more general predictive
57 model could be conceived, allowing the estimation of both operating conditions for gasification
58 processes and safety parameters.

59 In this paper, the pyrolysis/oxidation mechanisms of simple organic dusts (starch, cellulose) were
60 studied using a Godbert-Greenwald furnace and by collecting and analyzing the gases generated at
61 different temperatures. As the determination of a simplified mechanism and of pyrolysis/oxidation
62 kinetics will also be useful to assess the burning velocity, tests were also performed in a flame
63 propagation tube in order to estimate a laminar flame velocity. Finally, as it is the ultimate goal of
64 this research project, whose global approach will be detailed in section 2.1., the dust explosion
65 severity of these powders were also determined. Once the combustion model elaborated and
66 validated for cellulosic compounds, it would be extended for instance to lignocellulosic residues
67 and food waste, for process safety purposes as well as for the optimization of gasification processes
68 or combustion of biomass.

69

70 **2. Materials and methods**

71 *2.1 Global approach*

72 Although this publication focuses on assessing the kinetics of pyrolysis and combustion of an
73 organic powder, it seems important to present the overall approach of the research project aiming to
74 model dust explosions and to propose optimized procedures for determining safety parameters.
75 Indeed, knowledge of reaction kinetics is, especially for fine powders, the basis of explosion
76 severity assessment.

By using a modified Godbert-Greenwald and by varying the dust concentration, the residence time, the carrier gas (air or inert gases) and the temperature, simplified pyrolysis/combustion kinetics of a dust cloud can be proposed. Such mechanisms can be introduced and adapted to already-existing flame propagation models (Torrado et al., 2018) aiming at estimating the laminar flame velocity S_{uL}. Moreover, these experiments also lead to the identification of the combustion gases generated during a dust explosion, piece of information that may be requested during a risk assessment study. The laminar flame velocity can also be approached by using various experimental set-ups as a flame propagation tube (Santandrea et al., 2020). Therefore, both numerical and experimental approaches will lead to S_{uL}. From this step, this intrinsic parameter can be used to assess the turbulent flame velocity S_{uT} of a flame propagating in industrial facility, provided that the hydrodynamic parameters, in particular the turbulence intensity ν'_{rms} and scales, are known. Models relating S_{uL} to the explosion severity parameters (i.e. the maximum overpressure P_{max} and the maximum rate of pressure rise dP/dt_{max}) will be then tested and adapted to i) predict orders of magnitudes of Kst parameter, ii) propose a 'tailor-made' test protocol, alternative to standards ones, in order to determine the safety parameters more accurately.

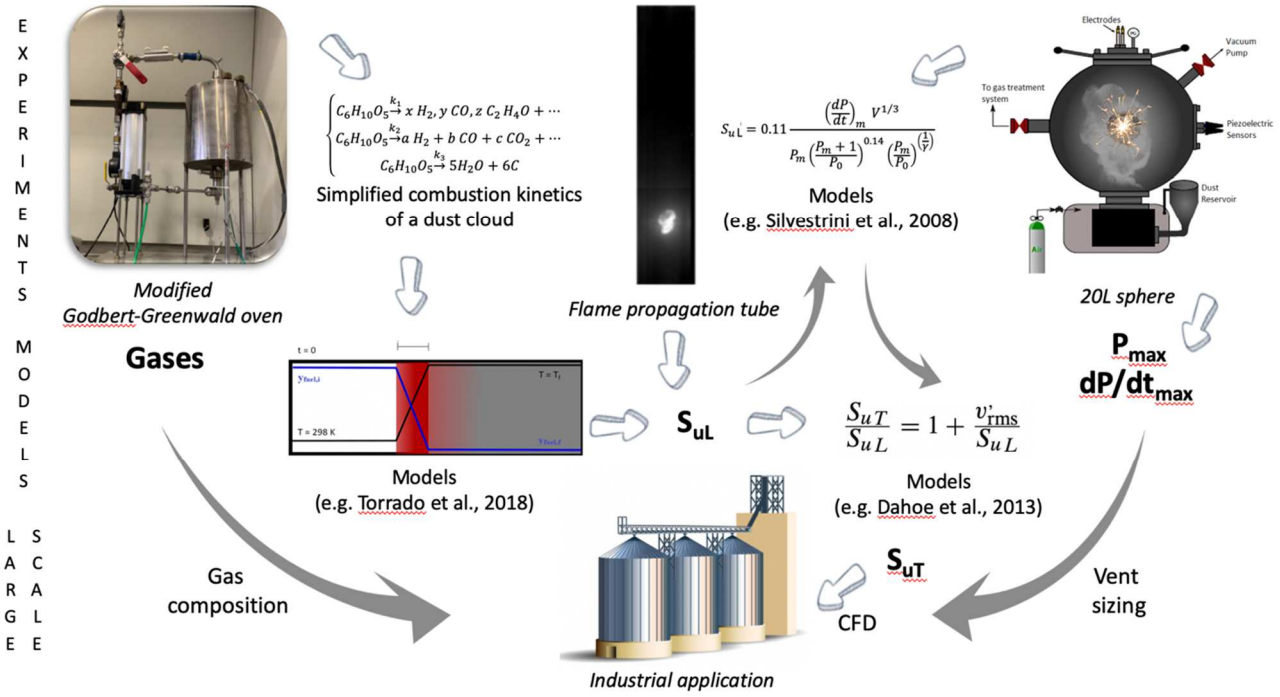

Figure 1. Descriptive diagram of the overall research project.

2.2 *Powders*

Tests were performed on two powders: wheat starch (Sigma-Aldrich) and cellulose (Arbocel, JRS). They both have the same monomer molecular formula ($C_6H_{10}O_5$, glucose), but show different structures. Indeed, in a starch chain, glucose molecules are linked to each other by means of a α(1-4) and a α(16) glycosidic chemical bonds, which gives this biopolymer its characteristic branched structure. On the other hand, in a cellulose chain, glucose molecules are kept together thanks to β(1-4) glycosidic bond, which leads to a more linear molecule. The choice of these two powders was dictated by the need to compare the combustion behavior of two different compounds having a quite similar chemical formula but different physical properties. Other organic molecules will be tested later, as well as mixtures of pure compounds in order to approach the phenomenon with several levels of complexity.

Table 1: Characteristics of the particle size distributions of starch and cellulose

Sample	d_{10} (µm)	d_{50} (µm)	d_{90} (µm)	SMD (µm)
Starch	9.8	22.3	42.1	18.5
Cellulose	14.4	53.3	196.0	33.3

Starch powder was sieved, initially in order to test the influence of the mean diameter on the combustion mechanism, but also to reduce its particle size distribution (PSD). In this paper, only the finest fraction will be studied. Table 1 shows the PSD of both samples and in particular the equivalent volume diameters d_{10}, d_{50}, d_{90}, and the Sauter mean diameter (SMD or $d_{3,2}$), i.e. the diameter of a sphere having the same volume/surface area ratio. The measurements were carried out by a laser diffraction sensor Helos (Sympatec) after dispersion of the dusts by an air-pulse in a semi-open tube. The dispersion procedure was consistent with that applied to determine the minimum ignition energy of a powder (ISO/IEC 80079-20-2). It should be noted that the PSD of starch is unimodal, which is not the case of cellulose. In fact, the cellulose sample is formed by

fibers of different shapes, lengths and geometric configurations. Their length-to-width ratios, estimated by optic microscopy, range from 6 to 10. A more thorough investigation of the time-evolution of the PSD of cellulose was carried out and shows three main peaks, at about 25, 60 and 190 µm (Figure 2). Except for the first 50 ms (absence of large agglomerates), the PSD remains stable for dispersion times up to 300 ms, which is noteworthy as ignition delay times ranging from 60 to 300 ms will be used to study the flame propagation.

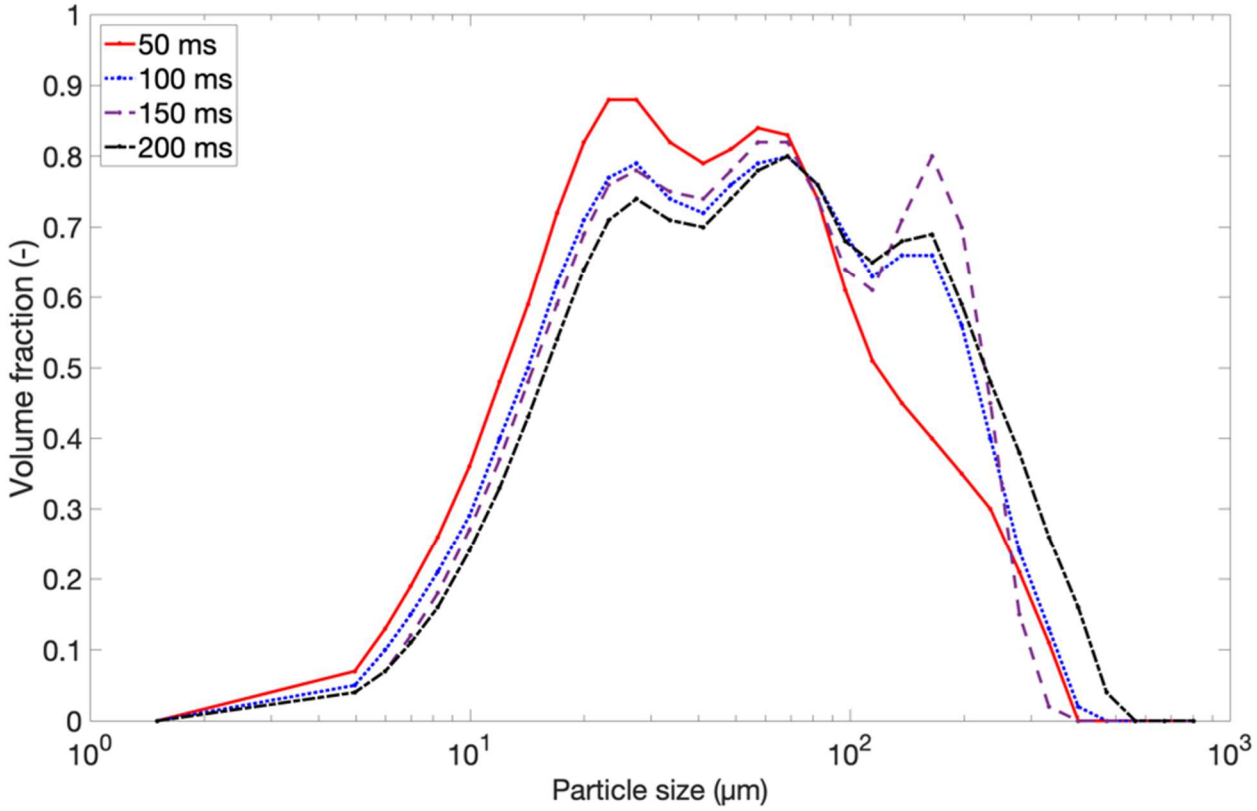

Figure 2. Time evolution of the PSD of cellulose for times ranging from 50 to 200 ms.

2.3 Analysis of the pyrolysis and combustion gases

Flash-pyrolysis and combustion experiments were carried out using a modified Godbert-Greenwald furnace, similar to the one used by Dufaud et al. (2012a).

The Godbert-Greenwald furnace is usually operated for the determination of the Minimum Ignition Temperature (MIT) of a dust cloud (ISO/IEC 80079-20-2). Due to its rather simple structure, bringing both benefits and drawbacks of standard procedures (Eckhoff, 2019), this apparatus is

versatile and suitable for other purposes (Azam et al., 2019; Bu et al., 2020; Tan et al., 2020). For instance, in this work, it is used as simple plug flow reactor. Because of its simple operating mode and its adaptability, this furnace provide the opportunity to study, among other things, the dynamics of a dust cloud generation, ignition phenomenon, particle heating process and consequent pyrolysis with generation of combustible gases.

As shown in Figure 3, the powder is dispersed into the vertical tubular furnace by a gas pulse (air for combustion and argon for pyrolysis). The emitted gases are then collected in a collapsible Tedlar bag situated at the bottom of the device and are analyzed with a micro gas chromatograph (µGC, Varian, CP 4900). Tests were performed thrice to obtain results with a good reproducibility degree.

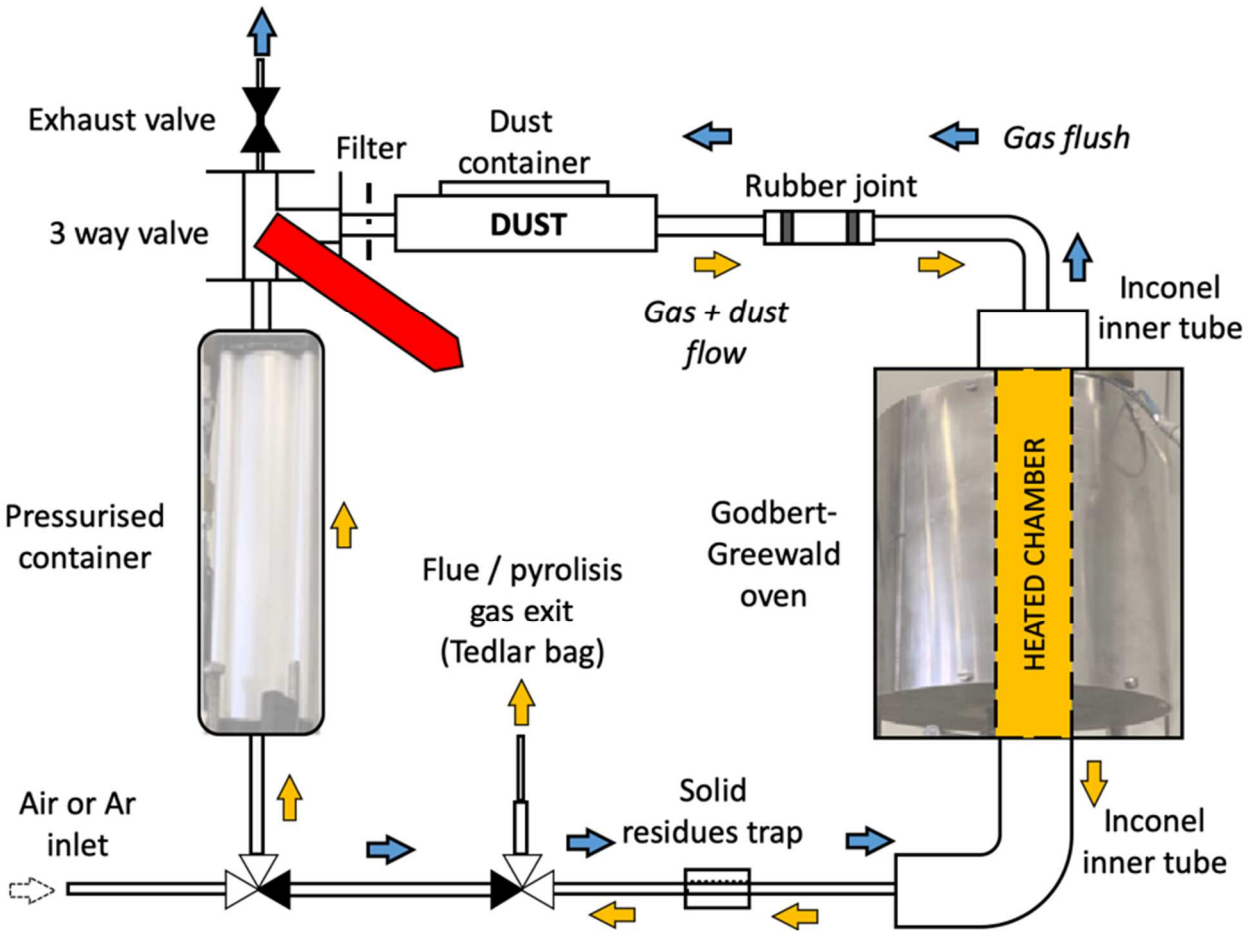

Figure 3. Scheme of the experimental setup used for the combustion and pyrolysis experiments

149 The pyrolysis and combustion products were determined at temperatures of 973 K, 1073 K and
150 1173 K, with masses of the samples varying between 0.1 g and 0.4 g and with an estimated
151 residence time of 200-250 ms. This time was determined by visualizing the powder entering and
152 exiting the furnace thanks to a high-speed video camera. For this study, the amount of powder was
153 set at 0.2 g, corresponding to a dust concentration in the Godbert-Greenwald furnace of
154 approximately 600 $g.m^{-3}$ (by considering a homogeneous dispersion of the dust in the oven
155 volume). It is much greater than both the minimum explosive concentration (approximately 60 $g.m^{-3}$)
156 (BGIA, 1997) and the stoichiometric concentration, as it leads to a theoretical fuel equivalence
157 ratio of 2.5. However, decreasing the dust weight will increase experimental uncertainties and
158 would not allow sufficient gas to be collected.
159 During the pyrolysis of organic powders, permanent gases, tar and char are generated (Nowakowska
160 et al., 2018). It should be underlined that, as the quantities of char and tar collected on small grids
161 placed at the bottom of the tube were very small with regard to the experimental reproducibility, no
162 reliable information could be obtained from such measurements. As a consequence, both
163 proportions will be deduced from a mass balance. An alternative design is under construction to
164 remedy such issues.
165
166 *2.4 Determination of the unstretched flame velocity*
167 Flame propagation tests were carried out in a modified Hartmann tube, which is a semi-open tube of
168 1 m long, with a square section of 7x7 cm^2 (Cuervo, 2015; Cuervo et al., 2017). The powder is
169 dispersed with a 7 bar compressed air pulse and then ignited with a 1 J electric spark. The
170 electrodes are 9 cm above the dispersion nozzle. The ignition delay time t_v, i.e. the time between the
171 dispersion and the ignition was set at 180 ms. This value results from a compromise between a high
172 t_v which ensures a weak turbulence of the dust cloud and a low t_v which avoids the segregation of
173 the particles (Figure 2). Tests were performed with 1 g of powder.
174 Flame propagation was recorded using a high-speed video camera (MotionBlitz EoSens mini2) and
175 a Matlab code developed by Cuervo (2015) was used to identify both the flame front position and

176 flame surface area. Then, assuming a linear relationship between the flame spatial velocity and the
177 stretching factor (Karlovitz factor) (Clavin, 1985; Markstein, 1964), the unstretched 'laminar'
178 burning velocity can be estimated (Cuervo et al., 2017).

179

180 *2.5 Dust explosion severity*

181 Experiments were performed using a standard 20L spherical vessel, equipped with a rebound
182 nozzle. Two 5 kJ chemical igniters were used as ignition sources in accordance with international
183 standards (EN 14034-1, 2004; EN 14034-2, 2006). The sphere was externally cooled with water at a
184 temperature ranging between 20 and 30°C. The maximum pressure P_m and maximum rate of
185 pressure rise, dP/dt_m, were determined for each test. The maxima of these parameters over a wide
186 range of concentration will be called P_{max} and dP/dt_{max}. Applying the 'cube-root law', the K_{st} index
187 will be deduced (Bartknecht, 1989).

188

189 **3. Results and discussion**

190 Two models were developed based on the experiments carried out on the Godbert-Greenwald
191 furnace: one representing the pyrolysis mechanisms, the other one, the combustion reactions, i.e.
192 the pyrolysis of the powder and the subsequent oxidation of the pyrolysis gases. They will be
193 described in this section, as well as the results of flame propagation and explosion tests performed
194 on cellulose.

195

196 *3.1 Model development for the pyrolysis of organic powders*

197 As previously said, during an organic dust explosion, the combustion of the powder occurs
198 following three main steps: first, the particle heating, then the pyrolysis/devolatilization and finally
199 the oxidation of the gases that have been produced by the pyrolysis. At this point, it is then
200 interesting to introduce the Damköhler number Da, which represents the ratio of the characteristic

diffusion time of the pyrolysis products (from the particle surface to the bulk of the gas phase) over the pyrolysis reaction time. The rate-limiting step of the process depends notably on the particle size distribution of the powder. In fact, the bigger the particles, the longer it will take for the two first steps to occur. When the oxidation in gaseous phase is very fast, three limitations can be considered as a function of the particle diameter and the external temperature. In Figure 4, four different pyrolysis kinetics have been considered (Chan et al., 1985; Di Blasi & Branca, 2001; Font et al., 1990; Wagenaar et al., 1993), but it should be stressed that they were usually obtained from thermogravimetric analyses or fluidized bed experiments (Cuervo, 2015). Therefore, it should be seen more as a qualitative approach than as a quantitative assessment of characteristic times. Considering the mean particle diameter of cellulose and starch powders used in this work and a temperature range of 973 to 1173 K, it can be seen that the pyrolysis mechanism is supposed to be mainly 'reaction-limited'. For very small particles, the oxidation can be the slowest step of the process. In this case, all the pyrolysis gases are emitted very quickly and will then react with oxygen to form the combustion products: the gas combustion is controlling the dust explosion (Di Benedetto et al., 2010).

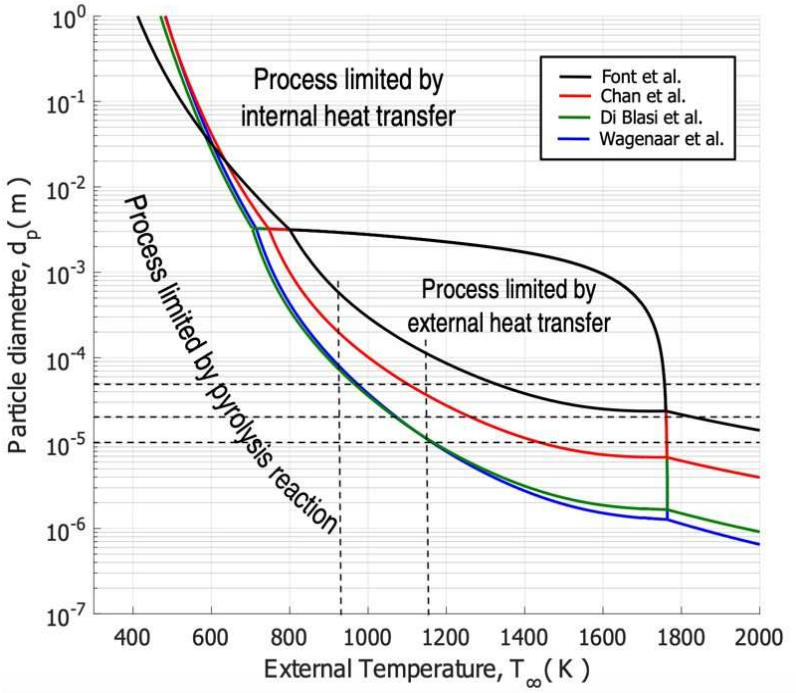

Figure 4. Regime limits as a function of the particle diameter d_p and the external temperature T_∞

219 It has been shown by Dufaud et al. (2012b) that, during a dust explosion, the critical particle size
220 corresponding to an intermediate regime (Da ≈ 1) for wheat starch is around 30 µm. Given the
221 significant influence of the pyrolysis step, two models were developed: a first one to predict the
222 pyrolysis products of organic compounds, which would then be implemented in a second model to
223 represent the distribution of their combustion products.

224 *3.1.1 Approach and assumptions*

225 A simplified model for the pyrolysis of organic compound was developed, whose aim is to predict
226 the proportions of the different species emitted during this process. The model was based on the
227 first experimental results carried out on starch dispersed in the furnace with argon, and is inspired
228 by the mechanisms of biomass pyrolysis developed by Ranzi et al. (2017). For simplicity purposes,
229 only three main reactions were considered to represent the emission of the pyrolysis products
230 (Equations 1- 3).

231 $$C_6H_{10}O_5 \xrightarrow{k_1} n_1H_2 + n_2CO + n_3CO_2 + n_4CH_4 + n_5C_2H_4 + n_6H_2O + n_7C_2H_4O \quad (1)$$

232 $$C_6H_{10}O_5 \xrightarrow{k_2} mH_2 + m_2CO + m_3CO_2 + m_4CH_4 + m_5C_2H_4 + m_6H_2O + m_7C_2H_4O \quad (2)$$

233 $$C_6H_{10}O_5 \xrightarrow{k_3} 5\,H_2O + 6\,C \quad (3)$$

234 It should be underlined that the purpose of this model was not to represent thoroughly the pyrolysis
235 phenomenon with all the gases potentially generated, but to present a simple alternative route based
236 on a few reactions which will be easily integrated in a more global model.

237 In this model, the two first equations represent the emission of the main pyrolysis gases as well as
238 water and acetaldehyde (C_2H_4O). This compound should be considered as a surrogate for the tars
239 and other permanent gases not considered here, rather than as acetaldehyde itself. Equations 1 and 2
240 are similar in their structure; but introducing this set of reactions in the model was necessary to
241 explain the evolution of the different gas concentrations as a function of temperature. Indeed,
242 experiments have shown that gas concentrations can either increase or decrease with temperature.
243 Considering a single equation and strictly positive activation energies, as proposed by Ranzi et al.

(2017), would only uniformly increase the gas concentration with temperature, which is inadequate. Equation 3 has been introduced to represent the formation of char (indicated as C in the reaction).

In addition to the simplification made on acetaldehyde generation, this model is based on the following assumptions: i) the pyrolysis takes place in an inert atmosphere (this has been verified as the amount of N_2, which would attest an air leak, was also analyzed by micro gas-chromatography), ii) both starch and cellulose are represented by the chemical formula $C_6H_{10}O_5$ and no impurity is present, iii) the powders are dried so there is no water inlet, iv) the reaction rate *i* can be written as:

$$r_i = k_i \, [C_6H_{10}O_5] \quad (4)$$

3.1.2 Solving method

A system of equations, based on the carbon, hydrogen and oxygen balances, was developed in order to determine the coefficients n_i, m_i and of the reaction rate constants k_i. It should be noted that the coefficients k_i are expressed using the Arrhenius law and depend on a pre-exponential factor A_i and an activation energy E_i. Rather than solving the system with the A_i and E_i as unknowns, which would introduce exponential functions, the coefficients n_i, m_i and k_i were determined for different temperatures. Then, the evolution of k_i as a function of the temperature allows the determination of A_i and E_i.

The concentrations of the following gases can be obtained directly through chromatographic measurements: carbon monoxide, hydrogen, carbon dioxide, methane and ethylene. By considering the furnace as a stirred tank reactor (or a succession of CSTR) and expressing the products concentration as a function of the carbon monoxide content, five ratios can be expressed as, for instance:

$$\frac{[H_2]}{[CO]} = \frac{n_1 \, k_1 + m_1 \, k_2}{n_2 \, k_1 + m_2 \, k_2} \quad (5)$$

It was unfortunately impossible to quantify precisely the amount of char and tar ; such metrology is currently developed. However, estimated values of two remaining ratios can be obtained by

applying atomic balances (C, H and O) to the experimental results, knowing the inlet dust concentration.

The system was solved using Matlab® with the function 'lsqnonlin', which is based on the resolution of a non-linear system of equations by the least square fitting. Lower boundaries were set to zero for the stoichiometric coefficients and the reaction rate constants. With regard to the results obtained by Ranzi et al. (2017), an upper limit of 10^{10} was set for the reaction rate constants.

3.1.3 Results of the pyrolysis tests

The results of the pyrolysis tests are presented in Table 2 for starch and cellulose for 973 and 1173 K. It should be noticed that carbon monoxide and hydrogen are the main gases (in molar proportions) produce by the pyrolysis, which is consistent with the literature (Commandre et al., 2011). Even if the orders of magnitude are close, differences are noticeable between the two products, especially at 973 K. For both powders, the CO/CO_2 ratio, hydrogen, ethylene and methane contents increase with the temperature. These trends are consistent with the shift of the C/CO_2 equilibrium towards CO when temperature increases. Moreover, the significant growth of hydrogen content for cellulose is not compensate by a decrease of methane, as methane conversion to hydrogen is made difficult by steam reforming (Commandre et al., 2011). Therefore, the evolution of hydrogen molar fraction is certainly due to water reaction. More generally, it should be noted that, even if they share the same monomer molecular formula, starch and cellulose do not show the same temperature-evolution of the pyrolysis gases.

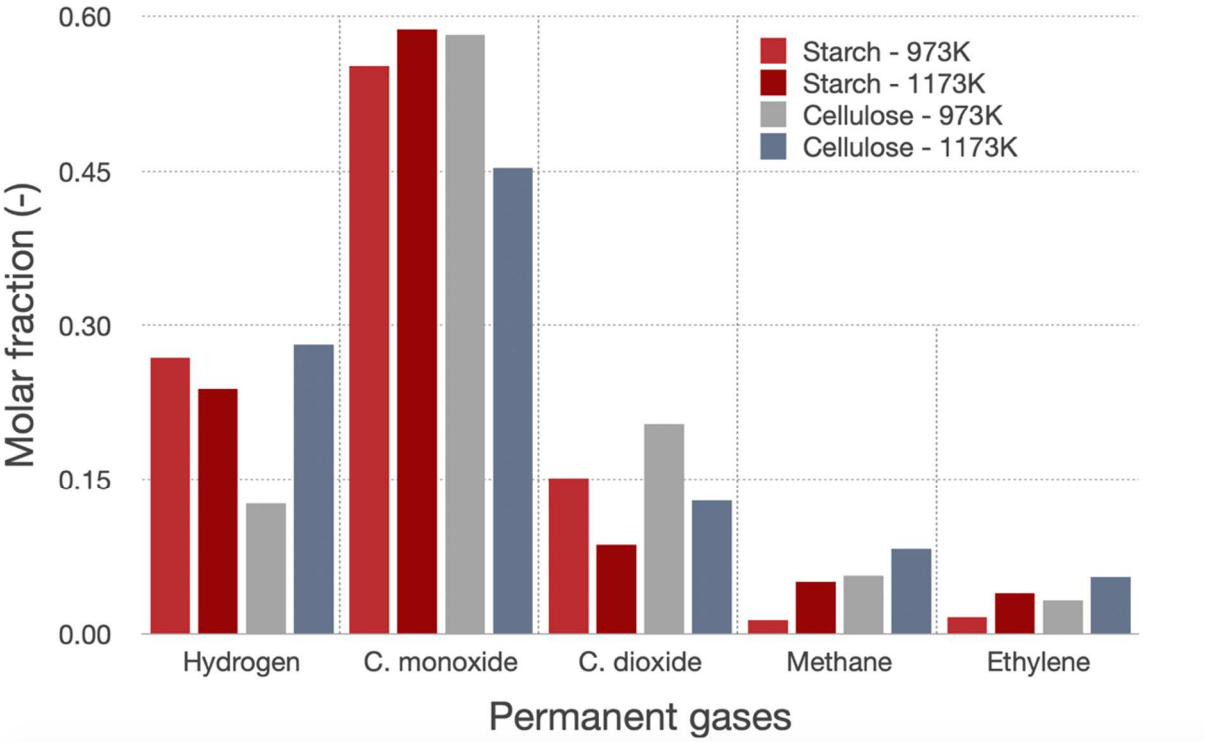

Figure 5. Permanent gases generated by pyrolysis of starch or cellulose (0.2 g) dispersed in argon at 973 and 1173 K

By applying atomic balances to the experimental results, the concentrations of 'char' (carbon), 'tar' (represented here by acetaldehyde) and water can be determined. For instance, for both starch and cellulose, the acetaldehyde concentration is approximately divided by 2 when the temperature increases from 973 to 1173 K: for starch, from 1.08 to 0.6 for the ratio $[C_2H_4O]/[CO]$. This trend is consistent with the fact that, at high temperatures, the final amount of tar is lower as it transforms into char and secondary gases. The water concentration seems to be rather constant for starch, but significantly decreases with temperature for cellulose, which can be coupled with the hydrogen production shown in Figure 5.

3.1.4 Results of the pyrolysis model

Using the resolution method previously described, the coefficients of the equations 1 and 3 have been determined as follows (Equations 6-7), for instance for wheat starch:

305 $$C_6H_{10}O_5 \xrightarrow{k_1} 1.17\ H_2 + 3.4\ CO + 0.02\ CO_2 + 0.45\ CH_4 + 0.32\ C_2H_4 + 0.83\ H_2O + 0.72\ C_2H_4O \quad (6)$$

306 $$C_6H_{10}O_5 \xrightarrow{k_2} 0.8\ H_2 + 1.7\ CO + 0.55\ CO_2 + 0.04\ CH_4 + 0.05\ C_2H_4 + 0.4\ H_2O + 1.83\ C_2H_4O \quad (7)$$

307 $$C_6H_{10}O_5 \xrightarrow{k_3} 5\ H_2O + 6\ C \quad (3)$$

308 The activation energies and pre-exponential factors of the three reaction rate constants k_i are shown
309 in Table 3. These values are in good agreement with those determined by Ranzi et al. (2017). It is
310 thus possible to predict the distribution of the pyrolysis products for any given temperature between
311 973 K and 1173 K. A verification has been performed by running the program at 1073K and
312 comparing the results with an additional set of experimental values. The composition of the
313 pyrolysis products calculated with the program can be seen in Figure 6. The gas concentrations
314 show a satisfactory match between the model and the experimental results, which tends to validate
315 the model, even if a deviation of nearly 30% can be observed for hydrogen.

316

317 *Table 3. Parameters of the reaction rate constants k_i determined for starch pyrolysis*

Reaction rate constants	Pre-exponential factor (s^{-1})	Activation energy ($kJ.mol^{-1}$)
k_1	1.2×10^{17}	318.6
k_2	8.8×10^{17}	41.0
k_3	2.8×10^{5}	72.6

318

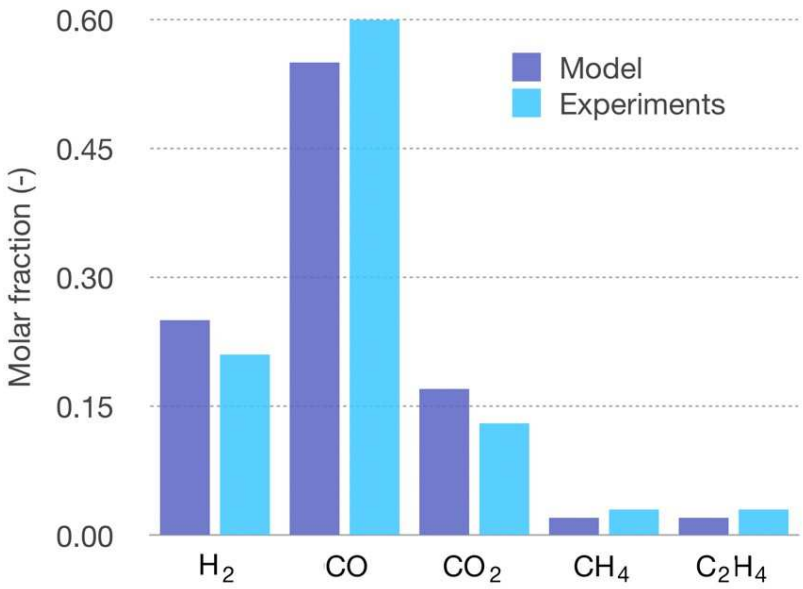

319

320 *Figure 6. Comparison between experimental and calculated gas molar fractions for starch at*

321 *1073 K*

322

323 The same development has been done for cellulose powder. Figure 7 shows the evolution of water

324 vapor, tar (represented by acetaldehyde), char and permanent gases for cellulose powder. As

325 observed for starch, the molar fraction of permanent gases increases with the temperature, whereas

326 both water and char contents globally decrease.

327

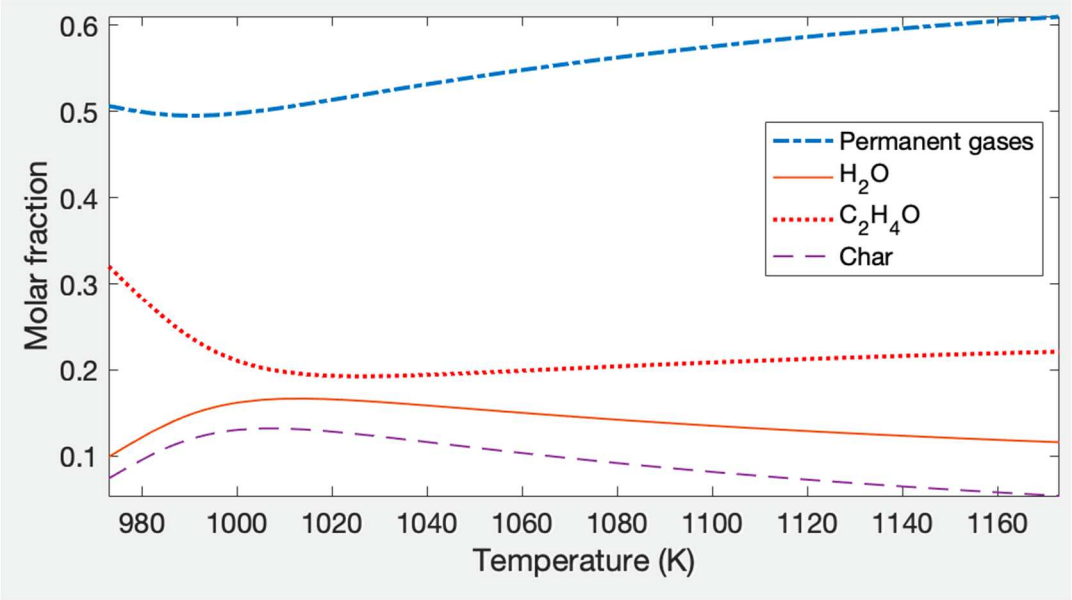

Figure 7. Evolution of the global composition of the pyrolysis products of cellulose from 973 to 1173 K

3.2 Model development for the combustion of organic powders

A similar approach has been used to model the combustion step. The results of combustion experiments performed in the Godbert-Greenwald furnace with air were used to fit two additional oxidation reactions (Eq. 8 and 9) complementing the global reaction mechanism.

3.2.1 Approach and assumptions

This model keeps all the reaction rate constants and coefficients calculated before and extends the two first pyrolysis equations into two supplementary equations with the addition of dioxygen to the pyrolysis products.

$$C_6H_{10}O_5 \xrightarrow{k_1} [pyrolysis\ products\ (pyr)]_1$$

$$[pyr]_1 + O_2 \xrightarrow{k_1'} n'_1H_2 + n'_2CO + n'_3CO_2 + n'_4CH_4 + n'_5C_2H_4 + n'_6H_2O + n'_7C_2H_4O \quad (8)$$

$$C_6H_{10}O_5 \xrightarrow{k_2} [pyrolysis\ products\ (pyr)]_2$$

$$[pyr]_2 + O_2 \xrightarrow{k_2'} m'_1H_2 + m'_3CO_2 + m'_6H_2O + m'_7C_2H_4O \quad (9)$$

$$C_6H_{10}O_5 \xrightarrow{k_3} 5H_2O + 6C \quad (3)$$

In addition to the assumptions done in section 3.1.1, this model is based on the following hypotheses:

i) the acetaldehyde produced during the pyrolysis reacts to form secondary gases; ii) all the char produced during the pyrolysis is a final product; iii) the char and water produced by the reaction (3) do not react with oxygen. Contrary to equations (1) and (2), (8) and (9) are not symmetric. Indeed, during the first stages of model validation, it appears that some stoichiometric coefficients were clearly negligible, allowing a simplification of reaction (9). To determine the new stoichiometric coefficients n', m' and the two reaction rate constants k'_1 and k'_2, the equation system has been solved using a method similar to that described in section 3.1.2.

3.2.2 Preliminary results of the combustion model

The stoichiometric coefficients are shown in equations 10 and 11. The values of the pre-exponential factors and activation energies are ($1.2.10^{17}$, 318.6 kJ.mol^{-1}) and ($8.8.10^{4}$, 41.0 kJ.mol^{-1}) for k'_1 and k'_2 respectively.

$$[pyr]_1 + O_2 \xrightarrow{k'_1} 1.35H_2 + 4.1CO + 1.09CO_2 + 0.45CH_4 + 0.34C_2H_4 + 1.67H_2O + 0.56C_2H_4O \quad (10)$$

$$[pyr]_2 + O_2 \xrightarrow{k'_2} 0.77\ H_2 + 4.19\ CO_2 + 2.15\ H_2O + 1.36\ C_2H_4O \quad (11)$$

The comparison between the model developed for the combustion of starch and the experimental results at 973 K, 1073 K and 1173 K can be observed in Figure 8. It shows a satisfactory agreement between the experimental data and the model, even if the differences are slightly larger at 973 K with a maximum deviation of 3%. It may also be noticed that the distribution of the gases varies less with temperature than during the pyrolysis step. Moreover, as expected, the concentration of carbon dioxide produced during the combustion (molar fractions of approximately 0.5) exceeds largely the amounts created during pyrolysis. Finally, the concentration of carbon monoxide is far from being negligible, which can be explained by the relatively high fuel equivalence ratio.

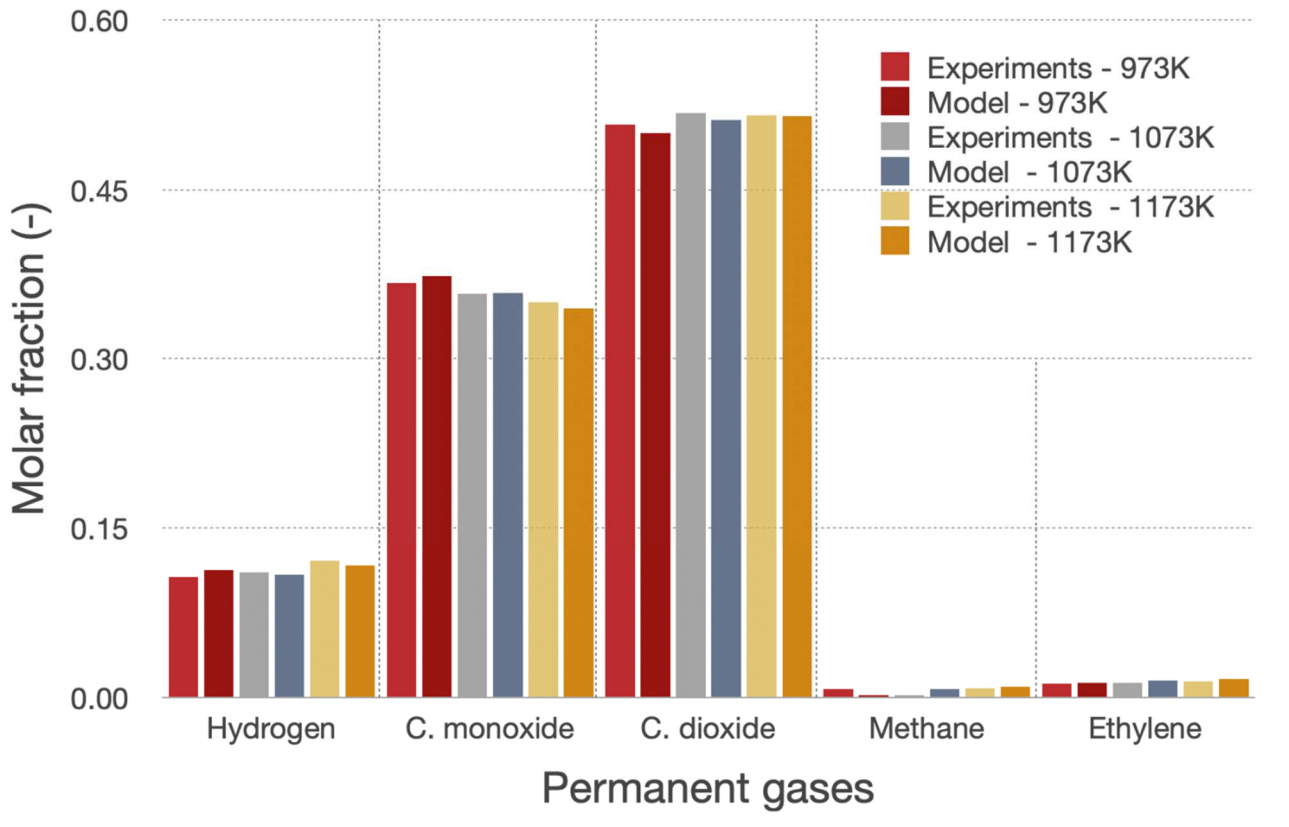

371

372 *Figure 8. Comparison between model and experimental data for starch combustion at 973 K,*

373 *1073 K and 1173 K.*

374

375 *3.3 Towards the determination of the burning velocity*

376 As said in section 2.1 and presented in Figure 1, such simplified mechanisms of a few lumped

377 reactions can be used to assess a laminar burning velocity (Torrado et al., 2018; Santandrea et al.,

378 2020). Therefore, the flame propagation of starch and cellulose in a semi-open tube was then

379 studied in order to determine a spatial flame velocity and estimate the laminar flame velocity. For

380 instance, Figure 9 illustrates the flame propagation of a cellulose dust cloud ignited by a 1 J spark.

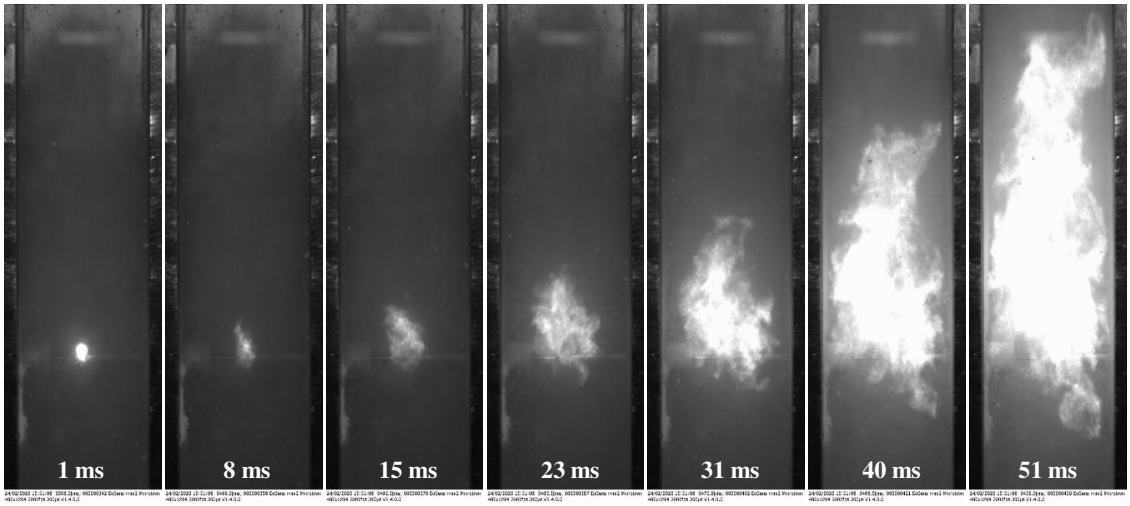

Figure 9. Flame propagation of a cellulose dust cloud. Ignition energy : 1 J, ignition delay time t_v : 180 ms, mass of powder : 1 g

Following the approach developed by Cuervo et al. (2017), the flame velocity can be plotted as a function of the Karlovitz stretch factor K, representing the time evolution of the flame surface area. K is defined as (1/A).(dA/dt), where A is the flame surface. Figure 10 shows that a linear trend can be observed for low stretching factors, the intercept corresponding theoretically to the laminar flame velocity of this cellulose/air mixture. A laminar flame velocity of 21.5 $cm.s^{-1}$ is obtained for the cellulose, which is in good agreement with the laminar burning velocity of nanocellulose determined by Santandrea et al. (2020), i.e. 21 $cm.s^{-1}$. Further tests should be performed to cover a wide range of conditions and the choice of a linear or non-linear regression to determine the intercept, and thus the laminar flame velocity, should be debated (Halter et al., 2010).

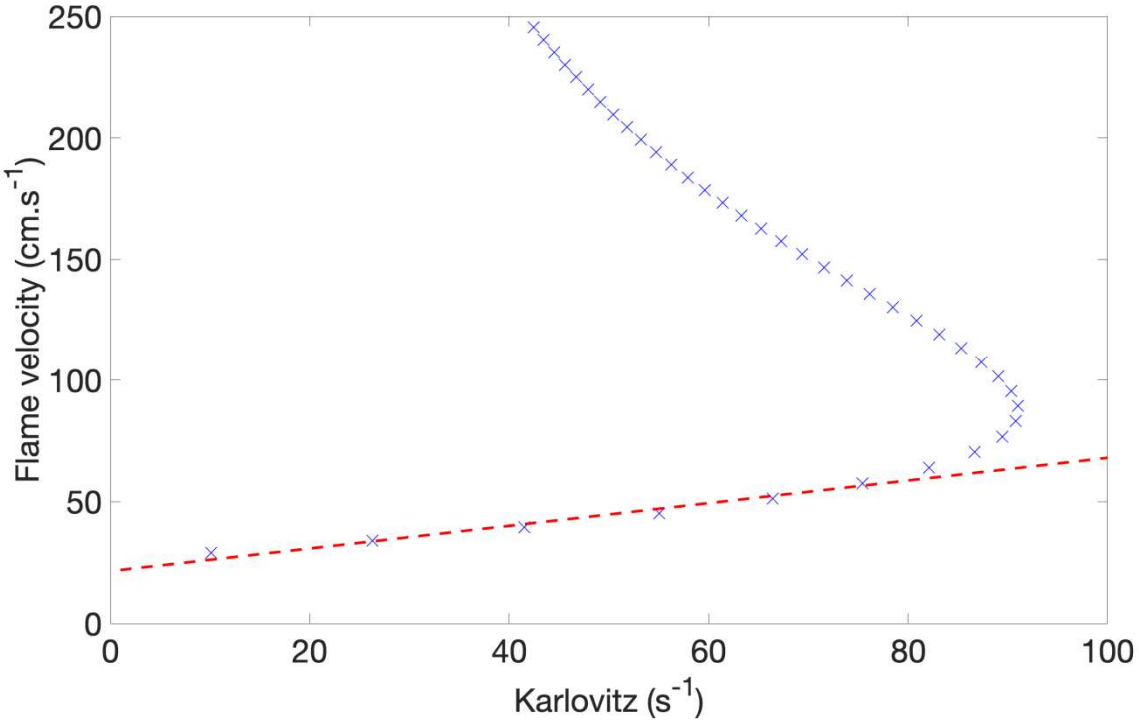

Figure 10. *Flame velocity versus stretching factor for a cellulose explosion. Ignition energy : 1 J, ignition delay time t_v : 180 ms, mass of powder : 1 g, d_{50} = 53 µm*

3.4 Explosion severity of organic powders

As notably shown by Figure 1, the final objective of proposing a simplified mechanism for the combustion of organic dusts is to model the explosion severity, especially the safety parameters usually determined under standard conditions in a 20L vessel. Preliminary tests were carried out to assess the maximum explosion pressure and maximum rate of pressure rise of cellulose (Figure 11). By considering the average values of three tests series, P_{max} reaches 6.8 bar, whereas $(dP/dt)_{max}$ is 287 bar.s^{-1}, which corresponds to a deflagration index K_{St} of 78 bar.m.s^{-1}. This latter parameter is consistent with the literature data for cellulose powder with a mean diameter ranging from 30 to 51 µm (BGIA, 1997) and with the value obtained for microcrystalline cellulose (d_{50} = 108 µm), i.e. 86 bar.m.s^{-1} (Santandrea et al., 2020). However, if P_{max} is slightly lower than the literature values for similar diameters, the whole PSD has to be considered (Figure 2) and additional tests should be performed between 500 and 1000 g.m^{-3}. This variation notably stresses the importance of taking into account all the operating parameters in order to determine safety parameters. Indeed, it seems

possible to optimize the test procedures (turbulence/ignition delay time-injection pressure, fuel equivalence ratio, ignition energy…) as a function of the powders characteristics.

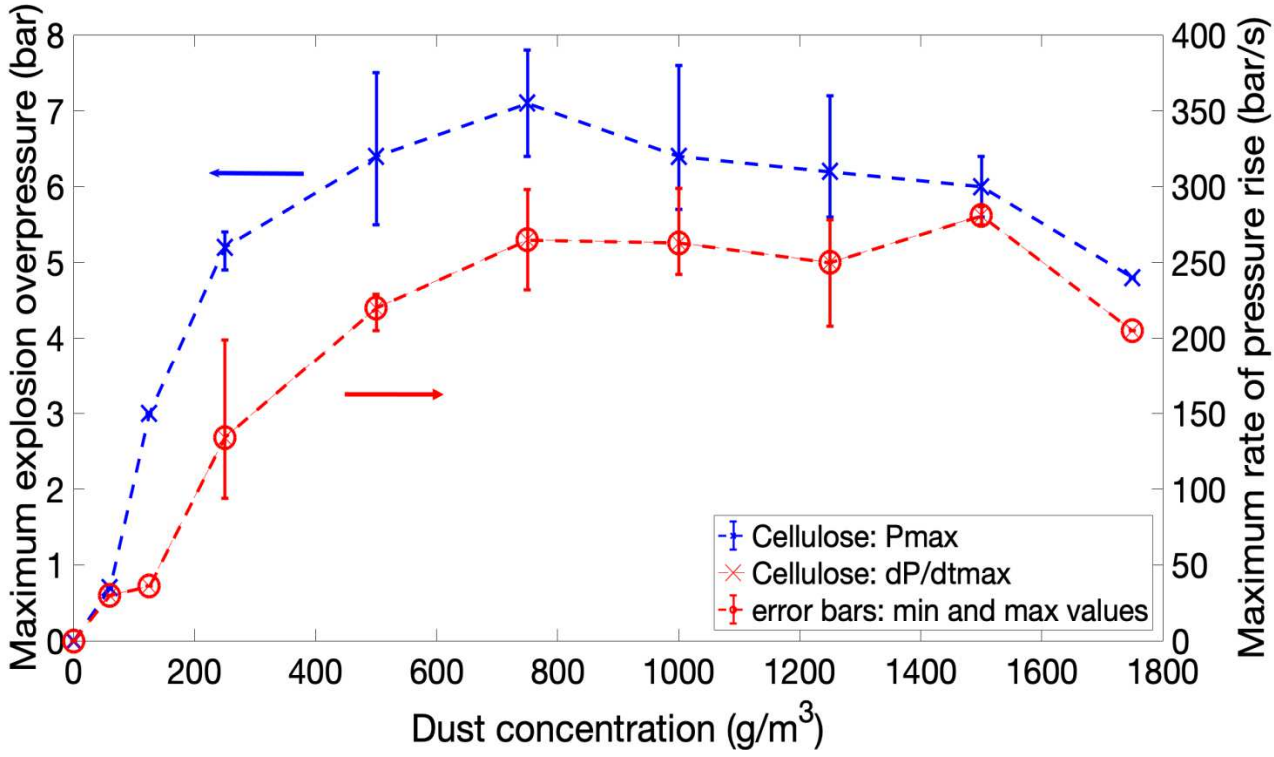

Fig. 11. Explosion severity of cellulose (d_{50} = 53 µm) determined with various series of experiments (the dotted line corresponds to an average trend).

4. Conclusions

During the explosion of organic powders, the particles undergo a pyrolysis process, emitting pyrolysis gases in quantities varying with the temperature. When mixed with oxygen, the oxidation reaction leads to heat generation and a flame propagation. Adapted to reactive systems with low Damköhler numbers, a semi-global mechanism has been developed to represent the pyrolysis of organic dust clouds. The model elaborated seems adequate to estimate the concentration of the different species considered, especially the permanent gases. Moreover, the molecule representing tar -i.e. acetaldehyde- has proven to be a satisfactory surrogate for modelling the cellulose pyrolysis. This model will be refined by better taking into account the 'char' generation, the influence of water and by studying the impact of the particle size distribution.

A second model, based on the oxidation reactions of tar and gases generated during the pyrolysis phase, has been proposed to represent reactive systems limited by the oxidation phase, i.e. for powders with small diameters. Although the first results are encouraging, the influence of the oxygen concentration or fuel equivalence ratio need to be further considered.

This study illustrates the predominance of particle structure over chemical formula and demonstrates that predictive dust explosion models must be adapted to the powder (and not only monomer) specificities. Once validated for starch, cellulose and mixtures of both products, the reaction mechanisms will be integrated in another existing model (Torrado et al, 2018) to estimate the laminar flame velocity of organic powders and, in a second time, to predict their maximum rate of pressure rise in a 20L sphere.

References

Azam, S., Mishra D. P. (2019). Effects of particle size, dust concentration and dust-dispersion-airpressure on rock dust inertant requirement for coal dust explosion suppression in underground coal mines, Process Saf. Environ. Prot., 126: 35-43. https://doi.org/10.1016/j.psep.2019.03.030

Bartknecht, W. (1989). Dust-explosions: Course, Prevention, Protection. Springer-Verlag, Berlin.

BGIA (1997). Combustion and explosion characteristics of dusts. BIA-Report 13/97 and Gestis Database, HVBG, Sankt Augustin, Germany.

Bu, Y., Yuan, Y., Xue, S., Amyotte, P., Li, C., Yuan, W., Ma, Z., Yuan, C., Li, G. (2020). Effect of admixed silica on dispersibility of combustible dust clouds in a Godbert-Greenwald furnace, Powder Technol. 374: 496-506. https://doi.org/10.1016/j.powtec.2020.07.071

Chan, W.C.R., Kelbon, M. & Krieger, B.B. (1985). Modelling and experimental verification of physical and chemical processes during pyrolysis of a large biomass particle, Fuel, 64(11):1505–1513. https://doi.org/10.1016/0016-2361(85)90364-3

Clavin, P. (1985). Dynamic behavior of premixed flame fronts in laminar and turbulent flows. Prog. Energy Combust. Sci., 11: 1–59. https://doi.org/10.1016/0360-1285(85)90012-7

457 Commandre, J.M., Lahmidi, H., Salvador, S. & Dupassieux, N. (2011). Pyrolysis of wood at high
458 temperature: The influence of experimental parameters on gaseous products. Fuel Process.
459 Technol., 92(5):837 - 844. https://doi.org/10.1016/j.fuproc.2010.07.009
460 Cuervo, N. (2015). Influences of turbulence and combustion regimes on explosions of gas-dust
461 hydrid mixtures (PhD Thesis). The University of Lorraine, France (in English).
462 Cuervo, N., Dufaud, O. & Perrin, L. (2017). Determination of the burning velocity of gas/dust
463 hybrid mixtures. Process Saf. Environ. Prot., 109: 704–715.
464 https://doi.org/10.1016/j.psep.2017.06.009
465 Di Benedetto, A., Russo, P., Amyotte, A., Marchand , N. (2010). Modelling the effect of particle
466 size on dust explosions. Chem. En. Sci., 65:772–779. https://doi.org/10.1016/j.ces.2009.09.029
467 Di Blasi, C. & Branca, C. (2001). Kinetics of primary product formation from wood pyrolysis. Ind.
468 Eng. Chem., 40(23): 5547–5556. https://doi.org/10.1021/ie000997e
469 Dufaud, O., Poupeau, M., Khalili, I., Cuervo, N., Christodoulou, M., Olcese, R., Dufour, A. &
470 Perrin, L. (2012a). Comparing pyrolysis gases and dusts explosivities: a clue to understanding
471 hybrid mixtures explosions? Ind. Eng. Chem., 51(22): 7656–7662.
472 https://doi.org/10.1021/ie201646s
473 Dufaud, O., Khalili, I., Cuervo, N., Olcese, R., Dufour, A., Perrin, L. & Laurent, A. (2012b).
474 Highlighting the importance of the pyrolysis step on dusts explosions, Chem. Eng. Trans.,
475 2012062, 369–374. https://dx.doi.org/10.3303/CET1226062
476 Eckhoff, R. K. (2019). Origin and development of the Godbert-Greenwald furnace for measuring
477 minimum ignition temperatures of dust clouds, Process Saf. Environ. Prot., 129: 17-24.
478 https://doi.org/10.1016/j.psep.2019.06.012
479 EN 14034-1, 2004. Determination of explosion characteristics of dust clouds — Part 1:
480 Determination of the maximum explosion pressure P_{max} of dust clouds.
481 EN 14034-2, 2006. Determination of explosion characteristics of dust clouds — Part 2:
482 Determination of the maximum rate of explosion pressure rise (dp/dt)max of dust clouds.

Font, R., Marcilla, A., Verdu, E. & Devesa, J. (1990). Kinetics of the pyrolysis of almond shells and almond shells impregnated with cobalt dichloride in a fluidized bed reactor and in a pyroprobe 100. Ind. Eng. Chem., 29(9): 1846–1855. https://doi.org/10.1021/ie00105a016

Fumagalli, A., Derudi, M., Rota, R., Snoeys, J., Copelli, S. (2018). A kinetic free mathematical model for the prediction of the K_{St} reduction with the particle size increase, J. Loss Prev. Process Ind., 52: 93-98. https://doi.org/10.1016/j.jlp.2018.02.002

Halter, F., Tahtouh, T., Mounaïm-Rousselle, C., 2010. Nonlinear effects of stretch on the flame front propagation. Combust. Flame 157, 1825–1832. http://dx.doi.org/ 10.1016/j.combustflame.2010.05.013.

ISO/IEC 80079-20-2, 2016. Explosive atmospheres — Part 20-2: Material characteristics — Combustible dusts test methods.

Liu, A., Chen, J., Huang, X., Lin, J., Zhang, X., Xu, W. (2019). Explosion parameters and combustion kinetics of biomass dust, Bioresour. Technol., 294: 122168. https://doi.org/10.1016/j.biortech.2019.122168

Markstein, G.H., (1964). Non-Steady Flame Propagation. Pergamon, New York.

Nowakowska, M., Herbinet, O., Dufour, A. & Glaude, P.A. (2018). Kinetic study of the pyrolysis and oxidation of guaiacol. J. Phys. Chem. A, 122 (39): 7894-7909. https://doi.org/10.1021/acs.jpca.8b06301

Ranzi, E., Debiagi, P.E.A. & Frassoldati, A. (2017). Mathematical modeling of fast biomass pyrolysis and bio-oil formation. Note I: kinetic mechanism of biomass pyrolysis. ACS Sustain. Chem. Eng., 5(4): 2867–2881. https://doi.org/10.1021/acssuschemeng.6b03096

Rathnayaka, S., Khan, F. & Amyotte, P. (2014). Risk-based process plant design considering inherent safety. Saf. Sci., 70:438-464. https://doi.org/10.1016/j.ssci.2014.06.004

Santandrea, A., Gavard, M., Pacault, S., Vignes, A., Perrin, L. & Dufaud, O. (2020). 'Knock on nanocellulose': Approaching the laminar burning velocity of powder-air flames. Process Saf. Environ. Prot., 134: 247–259. https://doi.org/10.1016/j.psep.2019.12.018

509 Scotton, M. S., Barozzi, M., Derudi, M., Rota, R., Copelli, S. (2020). Kinetic free mathematical
510 model for the prediction of K_{St} values for organic dusts with arbitrary particle size distribution,
511 J. Loss Prev. Process Ind., 67: 104218. https://doi.org/10.1016/j.jlp.2020.104218
512 Tan, X., Schmidt, M., Zhao, P., Wei, A., Huang, W., Qian, X., Wu, D. (2020). Minimum ignition
513 temperature of carbonaceous dust clouds in air with $CH_4/H_2/CO$ below the gas lower explosion
514 limit, Fuel, 264: 116811. https://doi.org/10.1016/j.fuel.2019.116811
515 Torrado, D., Pinilla, A., Amin, M., Murillo, C., Munoz, F., Glaude, P.-A. & Dufaud, O. (2018).
516 Numerical study of the influence of particle reaction and radiative heat transfer on the flame
517 velocity of gas/nanoparticles hybrid mixtures. Process Saf. Environ. Prot., 118: 211-226.
518 https://doi.org/10.1016/j.psep.2018.06.042
519 Wagenaar, B. M., Prins, W. & van Swaaij W.P.M. (1993). Flash pyrolysis kinetics of pine wood.
520 Fuel Process. Technol., Third international Rolduc symposium on coal science and technology
521 and related processes, 36(1): 291– 298. https://doi.org/10.1016/0378-3820(93)90039-7
522 Zhang, G., Zhang, Y., Huang, X., Gao, W., Zhang, X. (2020). Effect of pyrolysis and oxidation
523 characteristics on lauric acid and stearic acid dust explosion hazards, J. Loss Prev. Process Ind.,
524 63: 104039. https://doi.org/10.1016/j.jlp.2019.104039.